 doi:10.20944/preprints202108.0151.v1

Article

A Molecular Dynamics Simulations Study of the Influence of Prestrain on the Pop-in Behavior and Indentation Size Effect in Cu Single Crystals

Rong-Guang Xu[1*], Hengxu Song[2], Yongsheng Leng[1], and Stefanos Papanikolaou[3]

[1]*Department of Mechanical and Aerospace Engineering*

The George Washington University, Washington, DC 20052, USA

[2] *Institute for Advanced Simulations—Materials Data Science and Informatics (IAS-9), Forschungszentrum Julich GmbH, 52425 Julich, Germany*

[3] *NOMATEN Centre of Excellence, National Centre of Nuclear Research, A. Soltana 7, 05-400 Otwock, Swierk, Poland.*

* Correspondence: xrg117@gwmail.gwu.edu.

Abstract: The pop-in effect in nanoindentation of metals represents a major collective dislocation phenomenon that displays sensitivity in the local surface microstructure and residual stresses. To understand the deformation mechanisms behind pop-ins in metals, large scale molecular dynamics simulations are carried out to investigate the pop-in behavior and indentation size effect in undeformed and deformed Cu single crystals. Tensile loading, unloading and reloading simulations are performed to create a series of samples subjected to a broad range of tensile strains with/without pre-existing dislocations. The subsequent nanoindentation simulations are conducted to study the coupled effects of pre-strain, the presence of resulting dislocations and surface morphology, as well as indenter size effects on the mechanical response in indentation processes. Our work provides detailed insights into the deformation mechanisms and microstructure-property relationships of nanoindentation in the presence of residual stresses and strains.

Keywords: nanoindentation, avalanches, pop-ins

1. Introduction

Nanoindentation is a widely used technique to investigate mechanical responses of small volumes of materials at micro and nano length scales[1]. Indentation size effect (ISE), i.e., the hardness increases with the decreasing indentation depth (for sharp indenters) or with the decreasing indenter radius (for spherical indenters), opens up a new direction for the study of metal plasticity. The pioneering theoretical work dated back to 1998, Nix and Gao explained ISE by utilizing the concept of geometrically necessary dislocations (GND) to construct a mesoscale theory of strain-gradient plasticity based on the model of Taylor hardening[2]. One of the typical features of the plasticity at the small length scale is that the mechanical response (stress strain curve in uniaxial compression of pillar or force depth curve in nanoindentation) is intermittent. The intermittency is termed as pop-in in nanoindentation which is a displacement burst[3] in a load-controlled loading system or a force drop in a displacement-controlled loading system. The first pop-in event manifests the onset of plasticity and is believed to corresponding to the nucleation of dislocations in

 doi:10.20944/preprints202108.0151.v1

a confined dislocation-free volume, therefore, the shear strength when pop in events occur is thought to be close to the theoretical strength $G/2\pi$, where G is the shear modulus. However, it is found that as the indenter radius and pre-strain of the sample decrease, the first pop-in loads decrease and increase respectively, and the resulting maximum shear stresses derived from the pop-in loads increase[3,4]. This phenomenon exhibits another type of ISE: the stress required to initiate dislocation plasticity also depends on the size.

For the study of the crystal plasticity at the small length scale, molecular dynamics (MD) simulation has significant advantages: it can provide an atomistic picture of the loading process, offering many details of dislocation generation, propagation, reaction and annihilation[5-8]. MD simulations have been successfully performed and have made tremendous contributions in understanding various aspects of nanoindentation. However, most of previous MD studies were based on perfect crystal in which no preexisting dislocations existed in the simulation systems. In reality, dislocations cannot be ignored since even for well annealed metals, the dislocation density is in the range of 10^6-10^8 cm/cm^3. At the nanoscale, the role of existing dislocations is even more prominent, therefore, a defect-based model is needed to explain the real nanoindentation experiments. The effects of a variety of pre-existing defects such as vacancies, self-interstitial atoms and stacking fault tetrahedra (SFTs) on the incipient plasticity in dislocation-free metals have been reported[9,10]. The critical load decreases due to the presence of such defects. In a recent MD study[11], the indentation on a CaF_2 perfect crystal were performed in two steps. The first indentation was performed using a large indenter (R=12 nm) to induce plastic deformation, which is then followed by the second indentation with a small indenter (R=4 nm) performed in the middle of the pre-deformed zone. The interactions of pre-existing dislocations with the newly nucleated dislocations through the second indentation were studied. A smooth transition from elasticity to plasticity without a significant force drop was observed. In a similar study[12], plastic deformation was induced by nano-scratching with a 4 nm spherical tip, then the nanoindentation with a 3 nm spherical tip was carried out to assess the subsurface damage. Their simulations reveal that the maximum hardness decreases continuously with increasing machining depth of the surface, while the indentation hardness has no strong dependence on the prior nanomachining. In a more recent MD simulations[13], a single, two and three extended edge dislocation (EED) were introduced by removing one or more sets of two half layers of atoms. Subsequent MD simulations of nanoindentation investigated the mechanism of incipient plasticity in term of the mutual interaction of the existing dislocations. A newly published paper investigated the influence of pre-existing defects on hardness in nanoscale indentations, in which misfit dislocations was nucleated at semi-coherent Ti/Al bicrystal interface[14].

In this study, we introduce the dislocations in nanoindentation samples through a very natural manner by uniaxial straining a face-centered cubic (FCC) single crystal Cu to the plastic regime. This approach follows recent nanoindentation experiments that showed concrete effects of in-situ tensile loads on pop-in noise in Cu single crystals for depths up to 50nm[15]. Subsequent MD simulations of indentation are performed to explore the

 doi:10.20944/preprints202108.0151.v1

coupled effects of pre-strain, the presence of the resulting dislocations, and the indenter size on the mechanical response of the Cu single crystal.

The remainder of this paper is organized as follows. In Sec. II, the simulation method is described in detail. In Sec. III, we present detailed MD simulation results and discussion, followed by our summary in Sec. IV.

2. Materials and Methods

A substrate made of FCC single crystal Cu was initially constructed with $20 \times 20 \times 20\ nm^3$ in size and containing 702,464 Cu atoms. The x, y and z Cartesian axes are along the [100], [010], and [001] crystallographic directions, respectively (See **Fig. 1**). In the present work, we model the inter-atomic interactions between Cu atoms using standard interatomic potentials that provide an accurate description of a large variety of properties such as basic lattice properties, phonon frequencies, thermal expansion, diffusion, and equations of state for Cu[16].. All the simulations are performed using the LAMMPS (Large-Scale Atomic/Molecular Massively Parallel Simulator) open-source package (http://lammps.sandia.gov)[16].

Periodic boundary conditions (PBC) are implemented along directions (x and y directions) parallel to the indented surface to approximate the effect of one layer in the z direction that extend without bound in the x and y directions. For tensile pre-straining, the two (001) planes are free surfaces with zero traction. For indentation simulations, the bottom layers with thickness of 3 nm are hold fixed and atoms in the rest part of are free to move. In these simulations, temperature and pressure along x and y directions are maintained in equilibrium with a heat bath and mechanical reservoir using a Nosé–Hoover/Parinello-Rahman formalism[17-21]. Dynamic feedback between these reservoirs and the system allows the kinetic energy and volume to fluctuate about the desired mean values as expected in an equilibrium system. A time step of 1.0 fs is used throughout this investigation and the temperature of the simulating system is controlled at 10 K to avoid a temperature effect. The thermostatting and barostatting time scales are chosen to be 2 ps.

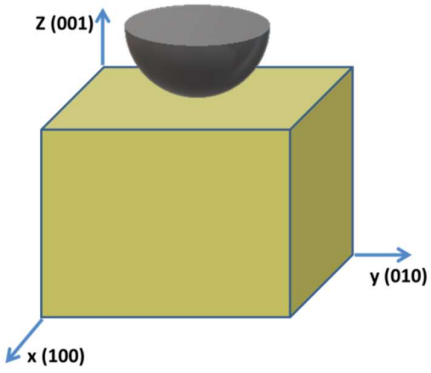

Fig. 1. Schematic representation of nanoindentation simulations. Indentations performed in (001) direction. The virtual indenter is represented by a nonatomistic rigid sphere. The nanoindentation spot is at (x = 10 nm, y = 10 nm).

Initially the substrate is relaxed under NPT ensemble control for 2 ns at 10 K and 0 GPa along x and y directions. Then, the substrate is deformed in the x direction at a constant strain rate of $10^9\ s^{-1}$ until strain = 0.6 is reached, during which the substrate undergoes elastic and then plastic deformations. Thus the dislocation distributions are created and stored in the Cu substrate. The subsequent nanoindentation simulations are then performed on the (001) surface of the system (See **Fig. 1).** The virtual indenter is

 doi:10.20944/preprints202108.0151.v1

represented by a nonatomistic rigid sphere with repulsive potential interacting with atoms in the substrate[5]. The form of such potential is adopted as

$$V(r) = \begin{cases} \frac{1}{3}k(R-r)^3, r < R \\ 0, \quad r \geq R \end{cases} \quad (1)$$

The indentation simulations were carried out in a displacement-control mode and the indenter is moving downward with a speed of 2m/s.

The indentation force F is calculated by the sum of the forces exerted by all atoms in the substrate on the indenter along z direction, i.e. vertical to the top surface. In order to obtain the variations of the hardness (here defined as the contact pressure) as a function of the indentation depth, it is crucial to calculate contact area properly. We followed the method in ref[22], where the elliptic contact area is calculate by $A^{elliptic} = \frac{\pi}{4}(x^{max} - x^{min})(y^{max} - y^{min})$, i.e. identifying four atoms in contact with the indenter which have the largest positive or negative x and y coordinates. Here x and y are the coordinates of the contact atoms projected into the initial surface plane.

According to the Hertzian solution[23], the maximum shear stress (τ_{max}) at pop-in can be obtained by $\tau_{max} = 0.31p_{max}$, where the maximum contact pressure is

$$p_{max} = \left(\frac{6FE^{*2}}{\pi^3 R^2}\right)^{1/3} \quad (2)$$

The relevant elastic parameters of Cu in the EAM potential are listed in TABLE 1,

Table 1. Elastic parameters of Cu in the EAM potential by Mishin et al.

	G (GPa)	ν	E (GPa)	E* (GPa)
Cu	47.8	0.3	129.1	147.1

The OVITO open visualization tool[24] is used to characterize the local structural environment of atoms by the common neighbor analysis (CNA)[25] and monitor dislocation movement[24]. The former can identify local crystalline structures of simple condensed phases formed by atoms ranging from FCC (face-centered cubic), HCP (hexagonal close-packed), BCC (body-centered cubic), SC (simple cubic), and ICO (icosahedral) to Other (unknown coordination structure). It can still work effectively in the presence of strong thermal fluctuations and strain. The latter can recognize all dislocations (including partial dislocation) in a crystal, determines their Burgers vectors, and output a line representation of the dislocation defects.

3. Results

3.1. Indentations on samples without pre-strain

As the first step, nanoindentation simulations are performed on the perfect crystal by four indenters with different tip radii. The indentation force-depth curves are shown in **Fig. 2**(a). For all cases, the substrate initially deform elastically until the first force drop. The data before the force drop can be fitted well to the Hertzian solution, i.e. a power-law relationship, $F \propto d^{3/2}$. The first force drops (also called pop-in load or critical load) are 0.04, 0.21, 0.38, and 0.60 μN for 1, 4, 7.5 and 15 nm indenter tips, respectively. And the corresponding indentation depths are 0.42, 0.77, 0.82, and 0.86 nm. The increase both in the critical force and depth with increase in the indenter tip size is due to the larger stressed volume with the larger tip radius, which is consistent with previous MD simulations[13].

Two types of the indentation size effect can be reproduced by measuring indentation hardness, pop-in load and corresponding maximum shear stress with different tip radius. Hardness-depth curves are shown in **Fig. 3**(a). Initially, the hardness curves increase with $d^{1/2}$-dependence before the drop, which are consistent with Hertzian elastic contact

Preprints (www.preprints.org) | NOT PEER-REVIEWED | Posted: 6 August 2021 doi:10.20944/preprints202108.0151.v1

solution. However, the large fluctuations in hardness associated with 1 nm indenter indicates its deviation because Hertz' analysis is valid only in the limit of d≪R. The hardness drops here are more pronounced than those in force-depth curves. After the drop, the hardness fluctuates roughly around a constant value, displaying noise that resembles bursts observed in generic nanomechanical studies[26,27]. As to indenter with 7.5 nm radius, its measured hardness is around 12 GPa, which agrees quite well with the previous simulation results[22]. More importantly, it should be noted that an increase in measured hardness corresponds to the decreasing indenter radius which is consistent with the conventional indentation size effect. As shown in **Fig. 3**(b), the pop-in load increases and the maximum shear stress decreases with increasing indenter radius, This is also referred to as the second type of indentation size effect[3] as mentioned above. It is not surprising that measurements based on maximum shear stress are consistent with those in terms of hardness.

Due to thermal fluctuations, the signal in force-depth curve is fuzzy. The energy-depth curves are smoother as shown in **Fig. 2**(b). As mentioned in Ref [10], the onset of plasticity for both the (111) and (110) orientations can be seen as a sudden drop in load, while pop-in in the (100) orientations is more gradual and sometimes is unobservable. In other words, dislocation nucleation can be viewed as a minor event, which is almost unobservable in the load-depth curves, before the major "pop-in" event. As explained in Ref[22], the slip system on (100) surface are more easily activated, since the corresponding Schmid factor of is 0.41 (while on (111) surface, it is 0.27). Also the (111) surfaces are mechanically stiffer so that larger plastic displacement jump would be observed when a considerable elastic energy has built up before dislocation avalanche happens. This confirms the claim by ref [28] that the indenter force is not a reliable indicator of the onset of plasticity. To identify the true incipient plasticity under nanoindentation, atomistic observations are required. In the following studies, the force drop will be identified by the associated energy drop combined with tracking of atomic events by visualization.

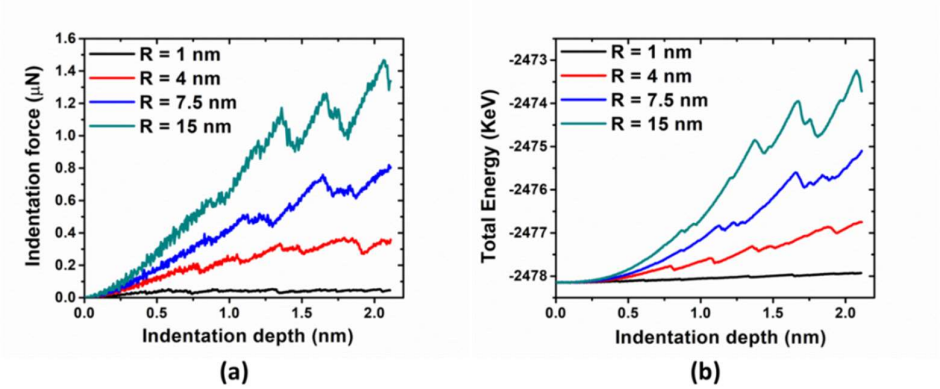

Fig. 2. (a) Indentation force and (b) total energy vs indentation depth for perfect crystal, indented with different tip radii.

 doi:10.20944/preprints202108.0151.v1

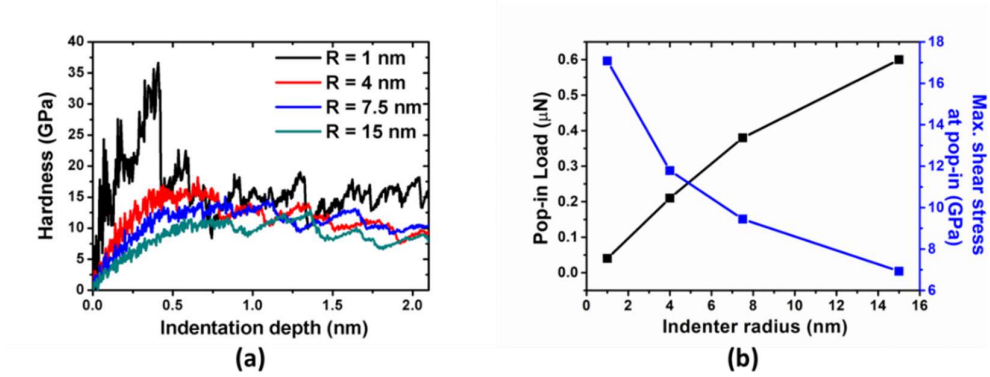

Fig. 3. (a) Hardness vs indentation depth with different tip radii, (b) Pop-in loads (black) and corresponding maximum shear stresses (blue) as a function of indenter radius.

3.2. Uniaxial tensile loading

Upon completion of 2 ns thermal equilibration process, the uniaxial tensile deformation is carried out at a constant engineering strain rate of 10^9 s^{-1} along x axis ([100] direction). The stress-strain behavior is shown in **Fig. 4**. This simulation is similar to the previous study on deformation behavior in <100> Cu nanowires[29]. Initially the sample undergoes elastic deformation along x direction with a linear increase in stress up to a peak value followed by a sudden drop. The flow stress fluctuates about 0.25 GPa without significant strain hardening. By detecting the formation and movement of dislocations, we find that the evolution of dislocation distribution is correlated with the observed stress-strain curve. As can be seen in the top-left inset figure, dislocation avalanche occurs when yielding, i.e. drastic drop in stress value is ascribed to nucleation of partial dislocation in an initially defect-free single crystal (In Cu, because of the low stacking fault energy, the partial dislocations dominate). The rapid decrease in dislocation density (dislocation depletion) with sharp decay of stress is believed to be ascribed to the fast movement of the dislocations to the sample free surfaces and annihilations. The lack of dislocation multiplication mechanism at such small length scale leads to dislocation starvation[30,31] because there is no chance that Frank-Read source would be activated due to its reduced dimensions.

Preprints (www.preprints.org) | NOT PEER-REVIEWED | Posted: 6 August 2021 doi:10.20944/preprints202108.0151.v1

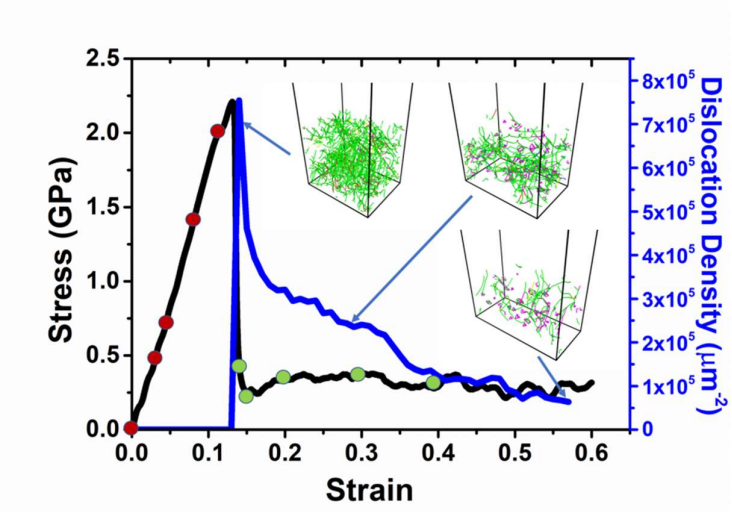

Fig. 4. Tensile stress-strain curve (black) and corresponding dislocation density (blue) during the uniaxial loading along x direction. The snapshots of dislocation distribution in substrate shown in inset figures. The red and green cycles represent samples with elastic and plastic deformation respectively where the subsequent nanoindentions will be conducted after thermal equilibration. Blue, green, pink, yellow, cyan and red lines represent perfect, Shockley partial, stair-rod, Hirth, Frank and other type of dislocations, respectively. The color scheme is consistent throughout this work.

3.3. Indentations on the samples with elastic deformation

Before indentation, the sample was hold at a constant strain for 500 ps to approach thermal equilibrium state, which is followed by subsequent nanoindentation (see in **Fig. 5**). In this scenario, there is no competing between pre-strain and existing dislocations and only pure strain effect comes into play. For a given indenter tip radius (R = 7.5 nm), the key characteristic of the pop-in (or critical) indentation load and depth decreases in general with an increase of the pre-strain (see in **Fig. 6**). While the pop-in size (the magnitude of force drop) generally increased with the pre-strain. For strain = 0.11, which are close to the yield point, the indentation force could drop abruptly to zero after elastic deformation. It can be concluded that in the elastic range, the nucleation of partial dislocation is much easier in the more pre-strained sample due to lower activation energy and bigger activation volume without the presence of preexisting dislocations.

Preprints (www.preprints.org) | NOT PEER-REVIEWED | Posted: 6 August 2021 doi:10.20944/preprints202108.0151.v1

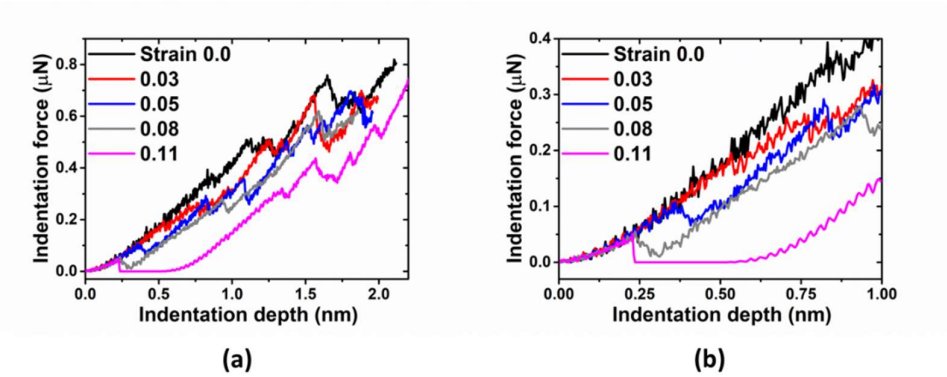

Fig. 5. (a) Indentation force vs indentation depth for Cu with elastic deformation, indented with tip radius R =7.5 nm. (b) Indentation force in the early stage of indentation.

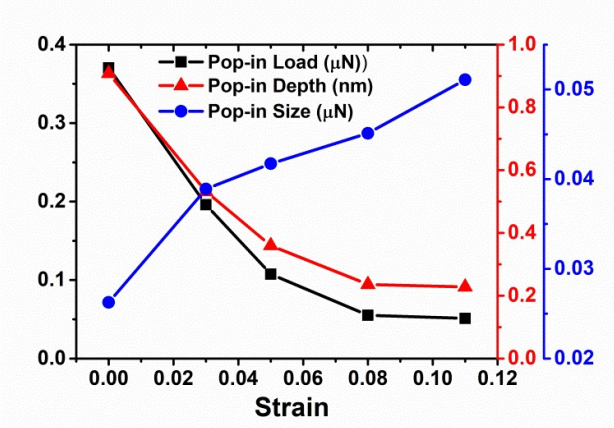

Fig. 6. The pop-in load, depth and size vs pre-strain for Cu with elastic deformation, indented with tip radius R =7.5 nm.

3.4. Indentations on the samples with plastic deformation

Before indentation, the samples were hold at constant strains for 500ps to approach thermal equilibrium state. **Fig. 7**(a) shows typical curves for evolution of different types of dislocations during such equilibrium process. As can be seen, the dislocation density decays very quickly to a plateau region. The initial and final snapshots of dislocation distribution in the sample are shown in insets in **Fig. 7**(a). The abovementioned dislocation starvation also occurs during the equilibrium process. **Fig. 7**(b) shows the equilibrium total and mobile dislocation density as a function of pre-strain. As the pre-strain increases, both of dislocation density decrease.

 doi:10.20944/preprints202108.0151.v1

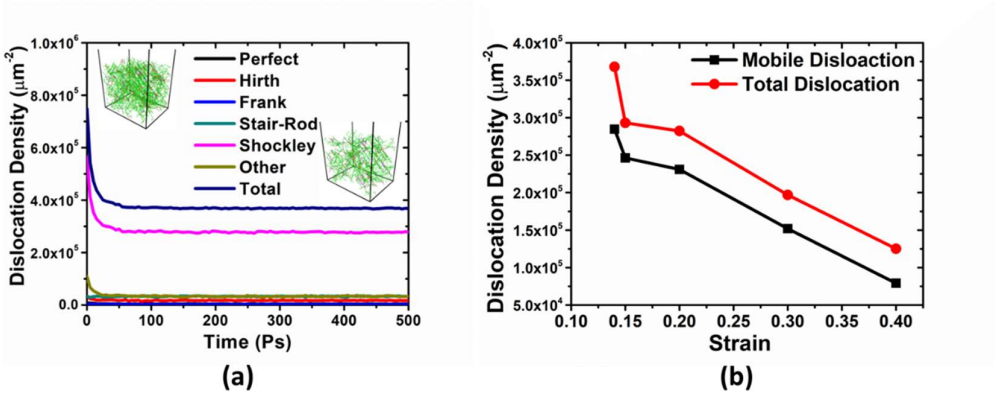

Fig. 7. (a) Evolution of different types of dislocations during 500 ps equilibrium run before nanoindentations for pre-strain 0.14. (b) The total and mobile dislocation density vs pre-strain.

In the next step, nanoindentation simulations are conducted. The indentation force-depth behaviors associated with different tip sizes are shown in **Fig. 8**. It should be noted that even initial deformations are not overlapped, which have been observed in previous study[12]. The pop-in loads and corresponding maximum shear stresses as a function of indenter radius with various strain levels are shown in **Fig. 9**. Compared with indentations on the samples with the elastic deformation, there is no distinct trend in this case. Especially for strain levels 0.2, the corresponding pop-in loads and maximum shear stresses are the lowest compared with other strain levels.

Preprints (www.preprints.org) | NOT PEER-REVIEWED | Posted: 6 August 2021 doi:10.20944/preprints202108.0151.v1

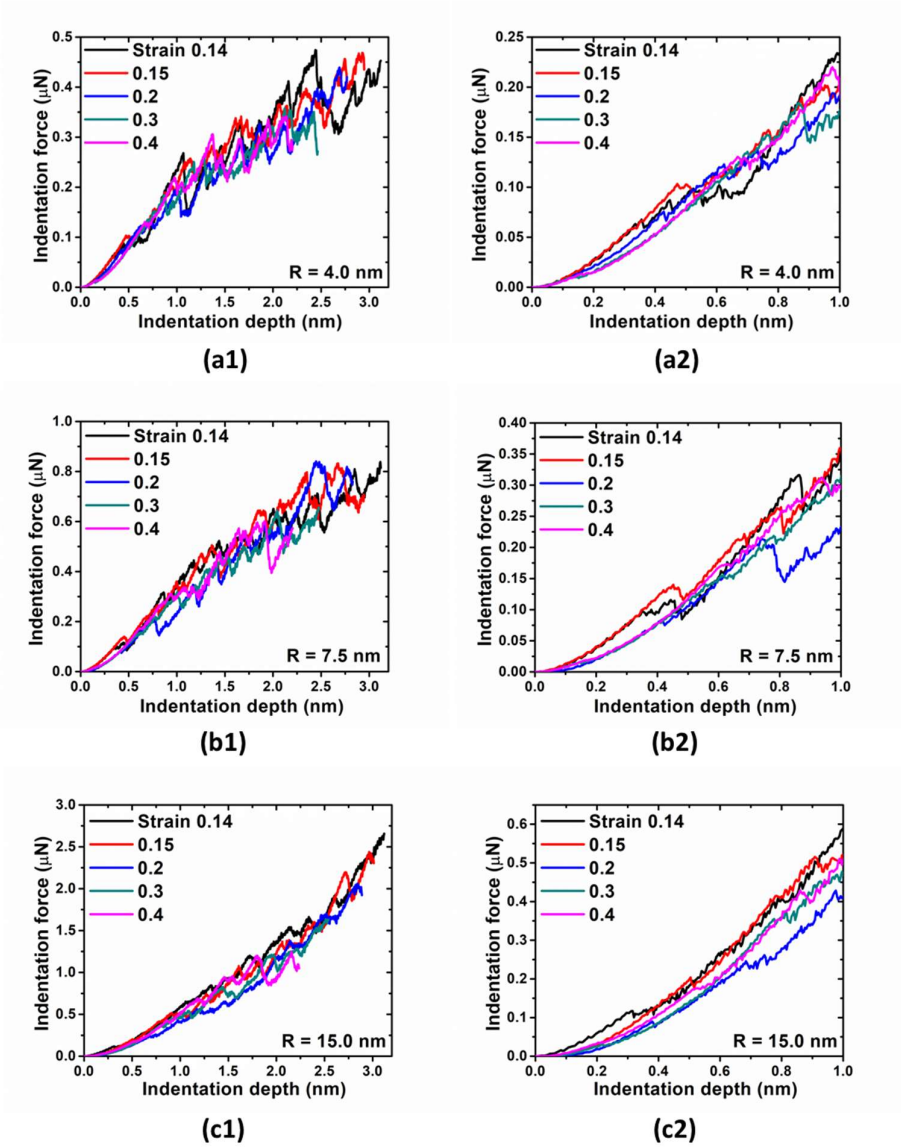

Fig. 8. Indentation force vs indentation depth for Cu under various plastic strain, indented with tip radius (a) R =4.0 nm, (b) R =7.5 nm, and (c) R =15.0 nm, respectively. Indentation force in the early stage of indentation is shown in the second column.

Preprints (www.preprints.org) | NOT PEER-REVIEWED | Posted: 6 August 2021 doi:10.20944/preprints202108.0151.v1

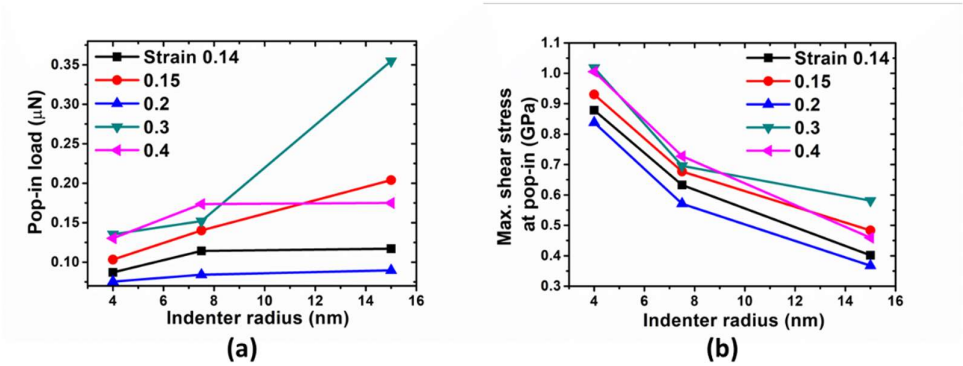

Fig. 9. (a) Pop-in loads and (b) corresponding maximum shear stresses as a function of indenter radius with various strain levels.

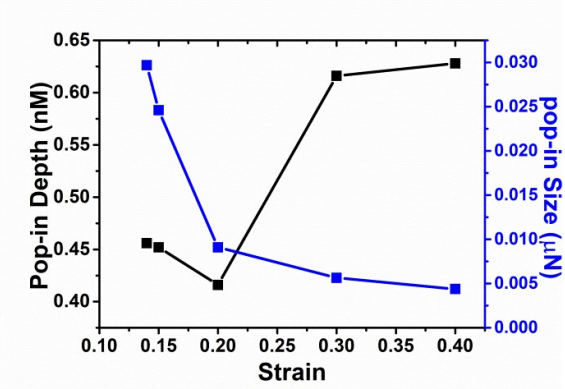

Fig. 10. The pop-in depth and size vs pre-strain for Cu with plastic deformation, indented with tip radius R =7.5 nm.

Let us take the sample indented with tip radius R =7.5 nm as a reprehensive examples. The variations of pop-in depth and size with the applied strain are also shown in **Fig. 10**, in which the pop-in size decreases with an increase of the pre-strain, while the pop-in depth in general increases with the pre-strain except strain level 0.2. Based on the atomic animations, we observe that these curves heavily depend on both the distribution of existing dislocation under the indenter and local morphology of substrate surfaces, although the nanoindentation spots (x = 10 nm and y = 10 nm as shown in **Fig. 1**) on the various samples are the same for each pre-strain. In other words, the specific distributions of existing dislocations and surface configuration induced by plastic deformation smear out the trend solely due to strain. It can be seen that the distribution of existing dislocation under the indenter and top surface morphology are quite different as shown in **Fig. 11**. It is found that five indentation simulations indented with tip radius R =7.5 nm under various pre-strains fall into three groups: (1) group 1 including smaller pre-strain (0.14 and 0.15) where load drops come from propagation of pre-existing dislocation underneath the indenter tip which is followed by dislocation nucleation under the tip, (2) group 2 including bigger pre-strain (0.3 and 0.4), where load drops result from the nucleation of dislocations from dislocation-free region under the tip while surrounding pre-existing

Preprints (www.preprints.org) | NOT PEER-REVIEWED | Posted: 6 August 2021 doi:10.20944/preprints202108.0151.v1

dislocations are not disturbed, and (3) group 3 including pre-strain 0.2, where the indenting is close to a surface step.

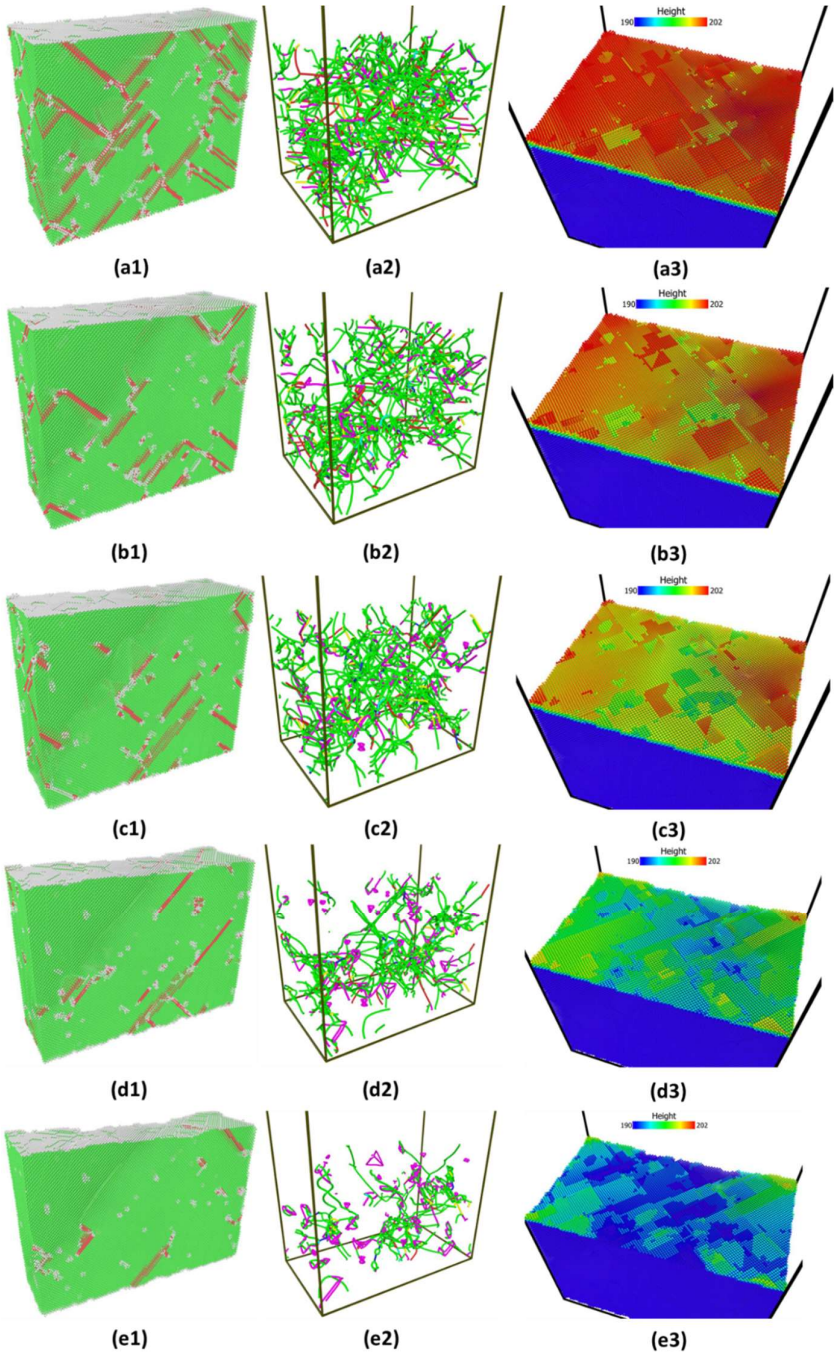

Fig. 11. Snapshots of initial atomic structure, distributions of dislocations and surface morphology before indentations at various strain levels (a1-a3) 0.14, (b1-b3) 0.15, (c1-c3) 0.2, (d1-d3) 0.3, (e1-e3) 0.4.

As the representative instances, the indentation force and total energy versus depth for two different strains (0.14 and 0.40) are shown in **Fig. 12**. Again, it can be seen that energy drop is a better indicator of incipient plasticity than the force drop. The evolution of atomic

Preprints (www.preprints.org) | NOT PEER-REVIEWED | Posted: 6 August 2021 doi:10.20944/preprints202108.0151.v1

structure and dislocations distributions marked by red cycles in both graphs of **Fig. 12** can provide detailed explanation for such different behaviors. **Fig. 13** shows that there exists a network of dislocations distributed across the sample under strain 0.14. As the indentation tip is pressed deeper and deeper (from **Fig. 13**(a) to **Fig. 13**(e)), the pre-existing dislocations are driven away due to the stress field induced by the tip (illustrated by the blue circles) as shown in **Fig. 13**(e), where there is no observable dislocation any more underneath the tip. It is followed by the nucleation of dislocations (a half loop) under the tip (see **Fig. 13**(f)). As to the strain of 0.40, on the other hand, nucleation of dislocations occurs (**Fig. 14**(d)) without any effect on the movement of surrounding dislocations. From **Fig. 14**(a) to **Fig. 14**(d), there are no observable rearrangements of distribution of pre-existing dislocations.

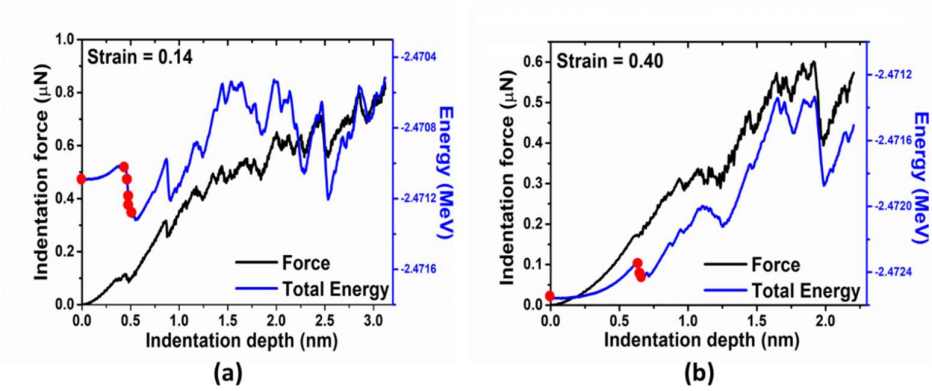

Fig. 12. Indentation force and total energy vs indentation depth for two different pre-strain indented with tip radius R =7.5 nm: (a) 0.14 and (b) 0.40. The detailed configurations associated with red circles are shown in **Fig. 13** and **Fig. 14**, respectively.

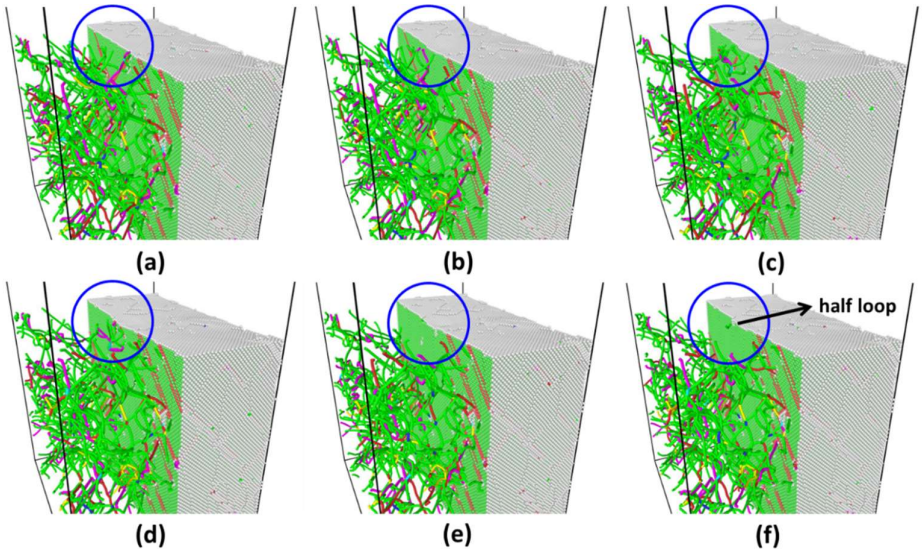

Fig. 13. Snapshots of atomic structure and distributions of dislocations across the sample under strain 0.14, which are corresponding to red circles marked in **Fig. 12**(a). The pre-existing dislocations are driven away due to the stress field induced by the tip (illustrated by the blue circles). (e) shows an half loop nucleated under the tip.

Preprints (www.preprints.org) | NOT PEER-REVIEWED | Posted: 6 August 2021 doi:10.20944/preprints202108.0151.v1

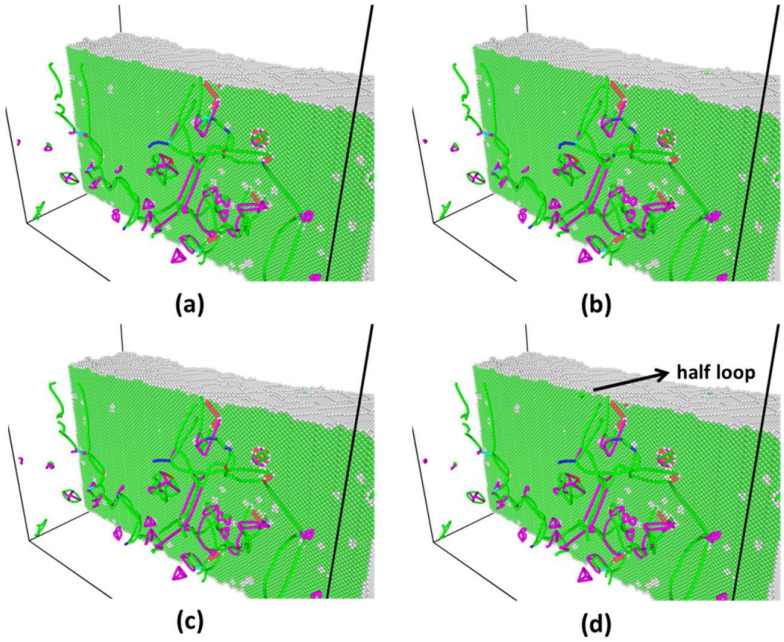

Fig. 14. Snapshots of atomic structure and distributions of dislocations across the sample under strain 0.40, which are corresponding to red circles marked in **Fig. 12**(b). (d) shows an half loop nucleated under the tip.

Plasticity can be initiated either by the activation of pre-existing mobile dislocations (strain = 0.14 and 0.15, see **Fig. 13**) or by the nucleation of dislocations (strain = 0.3 and 0.4, see **Fig. 14**). Obviously the latter requires higher stresses than the former. This is why we observe that at smaller strain (0.14 and 0.15) critical indentation load and critical indentation depth is smaller than that at the bigger strain (0.3 and 0.4). In the experimental work[3], they found that pre-straining measurably reduces the pop-in load due to the increasing initial dislocation density. A similar phenomenon was also found in the discrete dislocation dynamics study[32]. Our current study provides the same physical origin but shows different trend, which results from decreasing dislocation density with increasing pre-strain due to dislocation starvation in the small volume as discussed above.

The question remaining is why pop-in loads and corresponding maximum shear stresses with strain levels 0.2 are the lowest compared with other strain levels? It has been investigated by J. A. Zimmerman et al.[33] that the load required to nucleate dislocations decreases tremendously when indenting spot is close to the surface step. **Fig. 15** shows top surface morphology colored by height, in which the indenter center was positioned along black arrow. It is clear to see that the indenting spot is very close to a surface step, which can explain surprisingly low value of pop-in loads, depth and the corresponding maximum shear stresses.

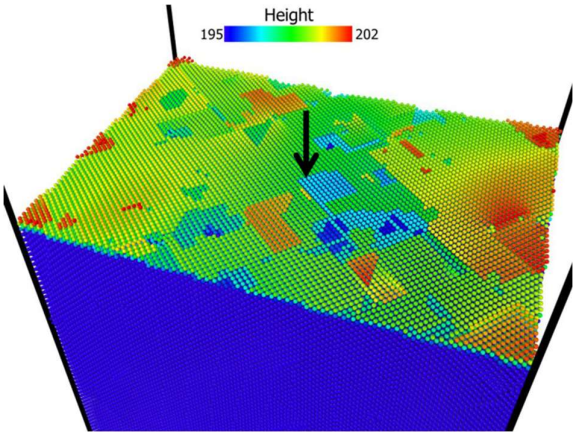

Fig. 15. Snapshots of initial surface morphology before indentations at the strain level 0.2. The black arrow represents positioning indenter center which is very close to a surface step. It should be noted that the indentation force curve heavily depends on where the indenter is located because both the distribution of existing dislocation and local morphology of substrate surfaces under the indenter is space-dependent. If a large number of indentation simulations can be done in many different spots and then the statistical analysis can be performed, the more precise relationship between pop-in loads and dislocation density can be established. This will be an open question and deserved to be investigated in the future studies.

3.5. Reloading and indentations on the samples with elastic deformation

To further investigate the competing effect between pre-strain and existing dislocations, we relax and unload the sample to zero stress from strain = 0.6. Then reload the sampling to locate yield point. The stress-strain behavior is shown in **Fig. 16**. Finally, the systems in such strain state as a certain percentage of yield stress are identified. Various pre-strain values are 0% (no pre-strain), 25%, 50%, 75% and 100% of the strain associated with yield stress. The subsequent nanoindentions are conducted with tip radius R =7.5 nm on various strain level after thermal equilibration.

Preprints (www.preprints.org) | NOT PEER-REVIEWED | Posted: 6 August 2021 doi:10.20944/preprints202108.0151.v1

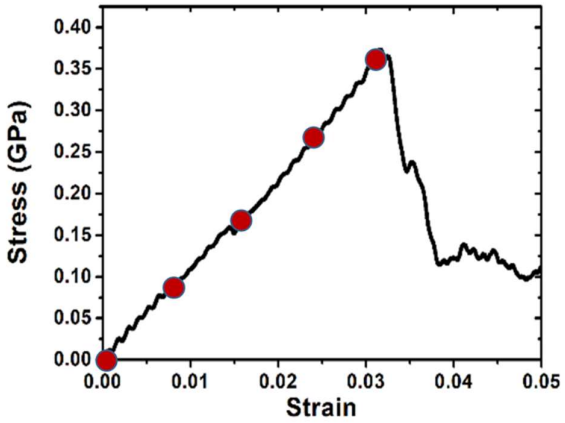

Fig. 16. Stress-strain curves in reloading process.

The indentation force-depth behaviors associated with different pre-strain are shown in **Fig. 17.** It can be seen that the trend in pure elastic strain (as in **Fig. 6**) recovers, i.e. increasing the pre-strain results in a decrease in the pop-in load and depth. But the pop-in size has no systematic variation.

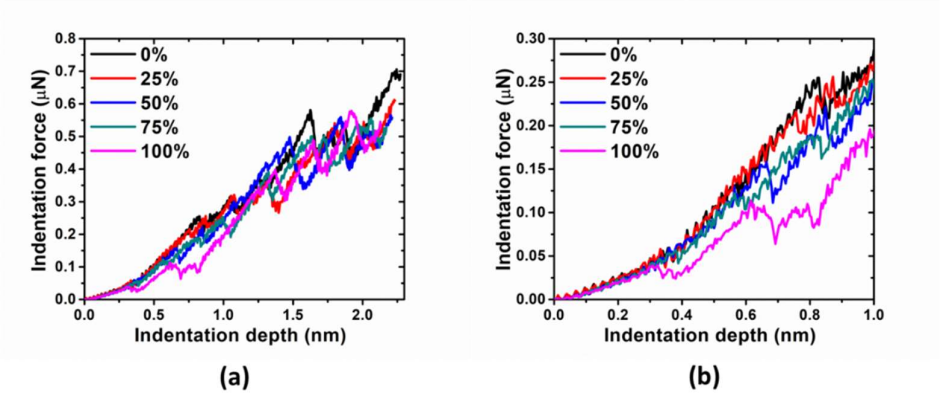

Fig. 17. Indentation force vs indentation depth with different pre-strains for Cu sample under reloading.

Preprints (www.preprints.org) | NOT PEER-REVIEWED | Posted: 6 August 2021 doi:10.20944/preprints202108.0151.v1

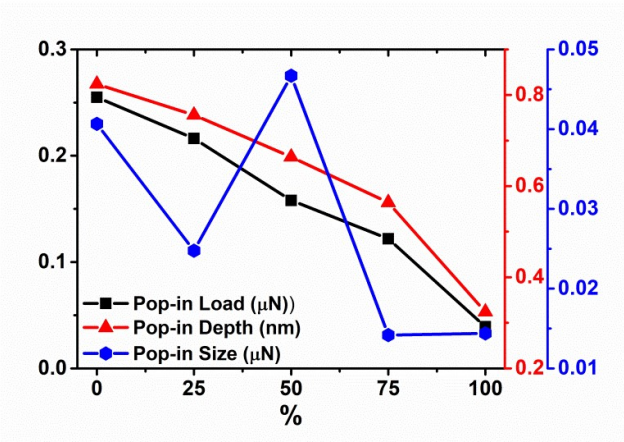

Fig. 18. The pop-in load, depth and size vs pre-strain for Cu sample under reloading, indented with tip radius R =7.5 nm.

Based on the atomic structures and distributions of dislocations as shown in **Fig. 19**, the dominating dislocation type is stair-rod, which is relatively immobile under stress. Furthermore, there is no much difference in the amount of mobile dislocation such as Shockley partial dislocations in various strain level. In this scenario, the strain effect would overshadow the effect of preexisting dislocations, which resemble case of the samples with elastic deformation in **Section C**.

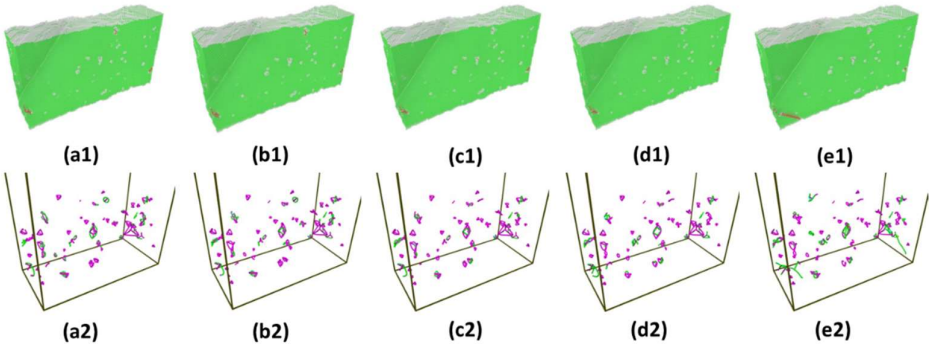

Fig. 19. Snapshots of initial atomic structures and distributions of dislocations before indentations at various strain level (a1-a2) 0%, (b1-b2) 25%, (c1-c2) 50%, (d1-d2) 75%, (e1-e2) 100%.

4. Conclusions

Through large scale MD simulations, nanoindentation of fcc single crystal Cu by a spherical indenter are performed to explore the coupled effects of pre-strain, the presence of resulting dislocations and surface morphology, and indenter size on the mechanical response in Cu substrate. We find:

(1) Two types of indentation size effects are reproduced in defect-free crystal. The trends of indentation hardness and maximum shear stress are consistent.

(2) During the indentation process, the total energy change is more sensitive to plastic deformation than the load change, which means that the indenter force is not a reliable

indicator of the onset of plasticity. Instead, the total energy of the system is a better indicator.

(3) In the elastic range, the nucleation of partial dislocation is much easier in more pre-strained sample due to lower activation energy and bigger activation volume without presence of pre-existing dislocations.

(4) Plasticity can be initiated either by the activation of pre-existing mobile dislocations (pre-strain = 0.14 and 0.15) or by the nucleation of dislocations (pre-strain = 0.3 and 0.4). The latter requires higher stresses than the former. So we observe that at smaller pre-strain (0.14 and 0.15) pop-in loads and the corresponding maximum shear stresses are smaller than that at the bigger pre-strain (0.3 and 0.4).

(5) The load needed to nucleate dislocations decreases tremendously when indenting spot is close to the surface step, which can explain surprisingly low value of pop-in loads and corresponding maximum shear stresses at pre-strain 0.2.

(6) After unloading and reloading to new yield point, subsequent nanoindentions conducted on various strain level show that the strain effect would overshadow the effect of preexisting immobile dislocations (stair-rod type), which resemble the case of the elastic strain.

Author Contributions: "Conceptualization, S.P..; methodology, R.G.X, H.S., S.P. ,Y.L..; software, R.G.X..; validation, R.G.X., S.P., Y.L., H.S..; formal analysis, R.G.X.; investigation, R.G.X..; resources, S.P.,Y.L.; data curation, R.G.X.; writing—original draft preparation, R.G.X..; writing—review and editing, S.P., Y.L., RGX, HS.; visualization, RGX; supervision, SP, YL.; project administration, SP, YL.; funding acquisition, SP. All authors have read and agreed to the published version of the manuscript.

Funding: We would like to acknowledge support from the EU Horizon 2020 research and innovation program (857470) and from FNP (MAB PLUS/2018/8), and acknowledge the computational resources provided by NCBJ.

Data Availability Statement: The data presented in this study are available on request from the corresponding author. The data are not publicly available due to privacy reasons.

Conflicts of Interest: The authors declare no conflict of interest.

References

1 Schuh, C. A. Nanoindentation studies of materials. *Materials today* **9**, 32-40 (2006).

2 Nix, W. D. & Gao, H. Indentation size effects in crystalline materials: a law for strain gradient plasticity. *Journal of the Mechanics and Physics of Solids* **46**, 411-425 (1998).

3 Papanikolaou, S., Cui, Y. and Ghoniem, N., 2017. Avalanches and plastic flow in crystal plasticity: an overview. *Modelling and Simulation in Materials Science and Engineering*, *26*(1), p.013001.

4 Shim, S., Bei, H., George, E. P. & Pharr, G. M. A different type of indentation size effect. *Scripta Materialia* **59**, 1095-1098 (2008).

5 Morris, J. R., Bei, H., Pharr, G. M. & George, E. P. Size effects and stochastic behavior of nanoindentation pop in. *Physical review letters* **106**, 165502 (2011).

6 Kelchner, C. L., Plimpton, S. & Hamilton, J. Dislocation nucleation and defect structure during surface indentation. *Physical review B* **58**, 11085 (1998).

7 Li, J., Van Vliet, K. J., Zhu, T., Yip, S. & Suresh, S. Atomistic mechanisms governing elastic limit and incipient plasticity in crystals. *Nature* **418**, 307 (2002).

8 Zepeda-Ruiz, L. A., Stukowski, A., Oppelstrup, T. & Bulatov, V. V. Probing the limits of metal plasticity with molecular dynamics simulations. *Nature* **550**, 492-495 (2017).

9 Salehinia, I. & Bahr, D. The impact of a variety of point defects on the inception of plastic deformation in dislocation-free metals. *Scripta Materialia* **66**, 339-342 (2012).

10 Salehinia, I., Lawrence, S. & Bahr, D. The effect of crystal orientation on the stochastic behavior of dislocation nucleation and multiplication during nanoindentation. *Acta Materialia* **61**, 1421-1431 (2013).

11 Lodes, M., Hartmaier, A., Göken, M. & Durst, K. Influence of dislocation density on the pop-in behavior and indentation size effect in CaF2 single crystals: Experiments and molecular dynamics simulations. *Acta Materialia* **59**, 4264-4273 (2011).

12 Zhang, J., Sun, T., Hartmaier, A. & Yan, Y. Atomistic simulation of the influence of nanomachining-induced deformation on subsequent nanoindentation. *Computational Materials Science* **59**, 14-21 (2012).

13 Ukwatta, A. & Achuthan, A. A molecular dynamics (MD) simulation study to investigate the role of existing dislocations on the incipient plasticity under nanoindentation. *Computational Materials Science* **91**, 329-338 (2014).

14 Chauniyal, A., Dehm, G. & Janisch, R. On the role of pre-existing defects in influencing hardness in nanoscale indentations—Insights from atomistic simulations. *Journal of the Mechanics and Physics of Solids*, 104511 (2021).

15 Bolin, R., Yavas, H., Song, H., Hemker, K.J. and Papanikolaou, S., Bending nano- indentation and plasticity noise in FCC single and polycrystals. *Crystals*, *9*(12), 652 (2019).

16 Plimpton, S. Fast parallel algorithms for short-range molecular dynamics. *Journal of computational physics* **117**, 1-19 (1995).

17 Nosé, S. A unified formulation of the constant temperature molecular dynamics methods. *The Journal of chemical physics* **81**, 511-519 (1984).

18 Nosé, S. A molecular dynamics method for simulations in the canonical ensemble. *Molecular physics* **52**, 255-268 (1984).

19 Hoover, W. G. Canonical dynamics: equilibrium phase-space distributions. *Physical review A* **31**, 1695 (1985).

20 Parrinello, M. & Rahman, A. Crystal structure and pair potentials: A molecular-dynamics study. *Physical Review Letters* **45**, 1196 (1980).

21 Parrinello, M. & Rahman, A. Polymorphic transitions in single crystals: A new molecular dynamics method. *Journal of Applied physics* **52**, 7182-7190 (1981).

22 Ziegenhain, G., Urbassek, H. M. & Hartmaier, A. Influence of crystal anisotropy on elastic deformation and onset of plasticity in nanoindentation: a simulational study. *Journal of Applied Physics* **107**, 061807 (2010).

23 Johnson, K. L. & Johnson, K. L. *Contact mechanics*. (Cambridge university press, 1987).

24 Stukowski, A. Visualization and analysis of atomistic simulation data with OVITO–the Open Visualization Tool. *Modelling and Simulation in Materials Science and Engineering* **18**, 015012 (2009).

25 Faken, D. & Jónsson, H. Systematic analysis of local atomic structure combined with 3D computer graphics. *Computational Materials Science* **2**, 279-286 (1994).

26 Papanikolaou, S., Dimiduk, D.M., Choi, W., Sethna, J.P., Uchic, M.D., Woodward, C.F. and Zapperi, S., Quasi-periodic events in crystal plasticity and the self-organized avalanche oscillator. *Nature*, *490*(7421), pp.517-521 (2012).

27 Song, H., Dimiduk, D. and Papanikolaou, S., Universality class of nanocrystal plasticity: Localization and self-organization in discrete dislocation dynamics. *Physical review letters*, *122*(17), p.178001 (2019).

28 Knap, J. & Ortiz, M. Effect of indenter-radius size on Au (001) nanoindentation. *Physical Review Letters* **90**, 226102 (2003).

29 Sainath, G., Rohith, P. & Choudhary, B. Size dependent deformation behaviour and dislocation mechanisms in⟨ 1 0 0⟩ Cu nanowires. *Philosophical Magazine* **97**, 2632-2657 (2017).

30 Greer, J. R. & Nix, W. D. Nanoscale gold pillars strengthened through dislocation starvation. *Physical Review B* **73**, 245410 (2006).

31 Brinckmann, S., Kim, J.-Y. & Greer, J. R. Fundamental differences in mechanical behavior between two types of crystals at the nanoscale. *Physical review letters* **100**, 155502 (2008).

32 Song, H., Yavas, H., Van der Giessen, E. & Papanikolaou, S. Discrete dislocation dynamics simulations of nanoindentation with pre-stress: Hardness and statistics of abrupt plastic events. *Journal of the Mechanics and Physics of Solids* **123**, 332-347 (2019).

33 Zimmerman, J., Kelchner, C., Klein, P., Hamilton, J. & Foiles, S. Surface step effects on nanoindentation. *Physical Review Letters* **87**, 165507 (2001).